

Direct Simulation Monte Carlo for astrophysical flows: II. Ram pressure dynamics

Martin D. Weinberg^{**}

Department of Astronomy, University of Massachusetts, Amherst, MA 01003-9305, USA

24 March 2021

ABSTRACT

We use the *Direct Simulation Monte Carlo* (DSMC) method combined with an n-body code to study the dynamics of the interaction between a gas-rich spiral galaxy and intracluster or intragroup medium, often known as the ram pressure scenario. The advantage of this gas kinetic approach over traditional hydrodynamics is explicit treatment of the interface between the hot and cold, dense and rarefied media typical of astrophysical flows and the explicit conservation of energy and momentum and the interface. This approach yields some new physical insight. Owing to the shock and backward wave that forms at the point ICM–ISM contact, ICM gas is compressed, heated and slowed. The shock morphology is Mach-disk-like. In the outer galaxy, the hot turbulent post-shock gas flows around the galaxy disk, while heating and ablating the initially cool disk gas. The outer gas and angular momentum are lost to the flow. In the inner galaxy, the hot gas pressurises the neutral ISM gas causing a strong two-phase instability. As a result, the momentum of the wind is no longer impulsively communicated to the cold gas as assumed in the Gunn-Gott (1972) formula, but oozes through the porous disk, transferring its linear momentum to the disk en masse. The escaping gas mixture has a net positive angular momentum and forms a slowly rotating sheath. The shear flow caused by the post-shock ICM flowing through the porous multiphase ISM creates a strong Kelvin-Helmholtz instability in the disk that results in Cartwheel-like ring and spoke morphology.

Key words: hydrodynamics — atomic processes — methods: numerical — galaxies: ISM, intergalactic medium — ISM: evolution

1 INTRODUCTION

The interaction between the intracluster medium (ICM) or the intragroup medium (IGM) and the interstellar medium (ISM) in a gas-rich spiral is often identified as the source of star bursts and gas starvation followed by morphological transformation. Recent observations of this process in the Virgo cluster have spawned a number of detailed hydrodynamic simulations that investigate the conditions required for these scenarios. This paper applies the hybrid Direct Simulation Monte Carlo (DSMC) method from Weinberg (2013, hereafter Paper 1) to the collision of two distinct gas components with different densities, temperatures and bulk velocities. Such an interaction is typically referred to as *ram pressure*. Many if not most ram pressure interactions are in the *transitional* regime which is not quite hydrodynamic. The subsequent evolution of the system depends on the dynamics at the collision interface and thereby provides a good test of the kinetic approach. Thus, the advantages

of DSMC all come to the fore when considering the ram-pressure mechanism and make ram pressure both a good problem for code comparison.

Although DSMC was developed for rarefied and transitional gas flows, the method has advantages for near continuum (i.e. low Knudsen number) flows: 1) there is no Courant-Friedrichs-Lewy (CFL) condition for DSMC; DSMC is unconditionally stable; 2) the method naturally resolves shocks without need for artificial viscosity or shock-capturing techniques; specifically, the inter-particle interactions on the mean-free-path scale are explicitly resolved and, therefore, there are no formal contact discontinuities; and 3) the DSMC approach naturally resolves the gas-phase interfaces that plague many hydrodynamic simulations when applied to scenarios with ISM cooling, e.g. giving rise to the *over-cooling* problem. The penalty for these advantages is much lower computational efficiency than the same computation using traditional grid hydrodynamics. This approach requires many more gas particles in the continuum limit than mesh cells or SPH particles, although it has the advantage of consistently transitioning from dense to dilute gases, fully

* E-mail: weinberg@astro.umass.edu

capturing shocks, and resolving phase boundaries. By design, DSMC is correct even as the mean free path becomes large. Such regimes are common in intracluster gas dynamics, hot bubbles and conduction at interfaces, and in multiphase ISM on small scales which require accurate treatment of interfaces. Moreover, this method maintains the underlying physics of the multiphase interfaces.

As the work proceeded, it became clear that the standard explanation of ram pressure did not explain results of the numerical experiments, either those described here or published elsewhere. To illustrate these differences, we will begin with the standard explanation for astrophysical ram pressure in Section 2, followed by an exploratory sequence of simulations of increasing generality in Section 3. These results will be compared with published observational and theoretical findings in Section 4. In brief, many of the features found here have been identified and reported by others (as expected for a code test) but the simulations here reveal a complexity of multiphase instabilities and angular momentum transport in the cold gas disk that has not been described previously. The overall explanation most commonly offered for this interaction is the ram-pressure paradigm envisioned by Gunn & Gott (1972, hereafter Gunn-Gott). However, we will argue that the dominant processes driving the evolution of a galaxy with a wind is not Gunn-Gott ram pressure but the combination of shock heating, boundary-layer ablation, Kelvin-Helmholtz instability in a multiphase medium, and angular momentum transfer. Because of this complexity, any specific observed interaction is likely to depend on the details of the galaxy, its gravitational environment and the density and speed of the wind. Owing to the expense of the DSMC method, we can not afford an exhaustive survey, but choose a single galaxy model and a high-density wind of modest to low velocity. In particular, we explore and describe the results for a one-dimensional slab, a three-dimensional disk + halo model with face-on, oblique, and edge-on winds, and include a case with and without a hot, coronal halo. We summarise in Section 5.

2 RAM PRESSURE

2.1 The astronomical setting

Galaxy clusters and groups are often permeated by hot, tenuous, X-ray emitting gas known as the intracluster medium (ICM). Throughout this paper, we will refer to both the intracluster medium and the intragroup medium (IGM) as the ICM. The pressure exerted by flows in this medium on a cold gas disk bound to the stellar disk is often described as ram pressure. In physics and engineering, ram pressure denotes the back pressure applied to a solid body moving through a fluid: $P = \rho v$ where P is the pressure, ρ is the mass density, and v is the relative speed of the body. Astronomers use *ram pressure* to denote the pressure applied by one fluid on another when the two fluids have distinct phases and significant relative bulk velocity. Let us refer to a hot tenuous gas that has significant bulk velocity with respect to the galaxy disk as a *wind*. *Ram pressure stripping* is said to occur if this wind is able to impart sufficient momentum to the cold disk that it overcome the gravitational attraction of the galaxy. Although we will retain the traditional terminology,

this paper will demonstrate that *ram pressure* is a physical misnomer in the astrophysical context; momentum transfer *does* occur, but it does not act like a macroscopic blunt body moving in a hydrodynamic flow. Rather, the details of the interaction of the two gas components with differing densities and temperatures is sufficiently dynamic that the ram pressure paradigm misses many of the essential features.

Regardless of the dynamical details, observational evidence for the interaction clearly exists. For simplicity, let us follow the standard practice of referring to the flow in hot medium relative to the frame of the cold galaxy as a *wind* and the resulting momentum transfer as *ram pressure*. Evidence for ram pressure can be found in many galaxy clusters. For example, three morphological features in NGC 4402¹ suggest strong gas interactions. First, the bowed morphology of the gas suggests a balance between the ram pressure and the lower gravitational force at larger disk radii. Secondly, the lower gas content in the extended blue stellar disk suggests a recent epoch of star formation, presumably induced by the interaction event. Finally, lanes of reddening can be seen trailing the inferred motion of galaxy in the cluster. The expected result of ram pressure stripping is a galaxy which contains very little cold gas. This effectively halts star formation in the galaxy, supporting the belief that ram pressure stripping could be one of the processes responsible for the morphology–density relation (see van der Wel et al. 2010, and references therein). Crowl et al. (2007) describe the observational case for ram-pressure stripping of NGC 4402 in detail.

Another interesting candidate is NGC 4522². Line-of-sight velocities suggest that this galaxy is currently falling towards the centre of the Virgo cluster (toward the bottom of the HST image²). The wind direction is less certain but presumably from below. The bowed and truncated disk, and the concentration of dust and gas to one side of the galaxy are all indicators that ram pressure stripping is forcing gas out of the galaxy. H-alpha images of this galaxy suggest that there is no gas in the outer disk, but there are gas filaments emerging from the plane of the disk, presumably caused by the interaction with the intracluster medium. The plume geometry of these features in NGC 4522 is consistent with predictions by the simulations described in Section 3.4 that post-shock gas will excite and then ooze through multiphase instabilities in the cold disk.

2.2 The Gunn–Gott ram-pressure criterion

We review the physical arguments for the classic Gunn–Gott ram pressure formula before moving on to the numerical experiments using DSMC in the next section. Consider a parcel of wind gas moving with respect the cold disk. The momentum per unit volume in the wind is

$$\text{wind momentum} = \rho_{ICM} v_{wind}. \quad (1)$$

The wind parcel crosses the stellar and gaseous disk in the time interval approximately given by h/v_{wind} . Therefore,

¹ Hubble image: <http://www.spacetelescope.org/images/heic0911c>

² Hubble image: <http://www.spacetelescope.org/images/heic0911b>

the momentum delivered by the stream of ICM parcels to the cold gas disk is

$$\text{wind force} = \rho_{ICM} v_{wind} \times \underbrace{v_{wind}/h}_{1/\text{duration}}. \quad (2)$$

The horizontally bracketed term in the equation above is the arrival frequency of ICM gas parcels, ignoring any dissipation. Finally, the condition that the volume force applied by the wind exceeds the gravitational restoring force binding the cold gas to the stellar disk is

$$\rho_{ICM} v_{wind}^2/h > \rho_{gas} \frac{\partial\Phi}{\partial z}. \quad (3)$$

Rearranging, we get a condition on the ram pressure required to strip the disk gas:

$$P_{ram} = \rho_{ICM} v_{wind}^2 > \Sigma_{gas} \frac{\partial\Phi}{\partial z}, \quad (4)$$

where $\Sigma_{gas} = \int dz \rho_{gas}(z) \approx \rho_{gas}(0)h$ is the gas surface density.

3 EXPERIMENTS

We will attempt to verify this physical picture with a short series of numerical experiments of increasing complexity. The numerical methods described in Paper 1 are briefly reviewed in the first section below and the initial conditions for the experiments are presented in Section 3.2. These are followed by in-depth descriptions of the one-dimensional (Section 3.3) and three-dimensional (Section 3.4) hot wind–cold disk simulations.

3.1 Methodology

DSMC solves the collisional Boltzmann equation when the collision term is dominated by two-body collisions for one or more species with or without internal degrees of freedom. Unlike molecular dynamics, the solution is obtained by sequentially computing the collisionless or *ballistic* flow followed by simulating the collisions implied by the Boltzmann collisional term. Essentially, the latter step is a Monte Carlo evaluation of the collision integral, and therefore a single simulation is one realisation of an ensemble of possible solutions. To help prevent the near-continuum limit from being a computational bottleneck, Paper 1 describes a hybrid DSMC approach that recovers the Navier-Stokes equation limit for mean free paths that are very small compared to any flow scale. This is achieved by limiting the number of collisions when the mean-free path becomes very small compared to any other scale of interest. In this limit, the solution in each collision cell is replaced by an equivalent thermalised randomly-generated distribution that conserves energy and momentum; this is called the Equilibrium Particle Simulation Method (EPSM, Pullin 1980; Macrossan 2001). The hybrid DSMC-EPSM algorithm was parallelised and merged with a collisionless N-body solver called EXP. Paper 1 demonstrates that this code correctly reproduces the standard shock-tube tests and develops Kelvin-Helmholtz instabilities following the analytic dispersion relation.

In the simulations below, the stellar disk and dark matter halo are self-gravitating and mutually interacting. The

gas feels the gravitational field generated by the stellar and dark matter components but do not exert gravitational force on these components or on itself. Therefore, in these runs, the gas cannot be gravitationally unstable. This is *not* a fundamental limitation of the combined EXP-DSMC code. For example, EXP also includes a PIC-Fourier Poisson solver that could be used to investigate the small-scale gravitational response of the gas to the momentum transfer from the wind. Rather, because the gravitational instabilities in the gas are likely to be on a much smaller scale than those of the stellar and dark matter components and because the mass in diffuse gas is very small compared to the mass in the stellar disk or halo, we choose to focus on the large-scale features of the flow. A simulation with a coronal halo is briefly described in Section 3.6; the heat generated by the wind interaction is sufficient to prevent the coronal gas from cooling. All of the DSMC simulations described here are fully three-dimensional, even though the initial conditions and gravitational Poisson solver have explicit symmetries.

3.2 Initial conditions

The first set of experiments (described in detail in Section 3.3) explores a one-dimensional wind interaction with a slab of cold gas confined by stars and dark matter. A planar stellar slab is realised from the exact isothermal solution to the equations of hydrostatic equilibrium. In the second set of experiments (Section 3.4), the stellar disk and halo are initialised as described in Holley-Bockelmann et al. (2005). In brief, the steps in realising the phase-space distribution for the second set of simulations are as follows: 1) the dark halo distribution function is realised by the Eddington inversion method (e.g. Binney & Tremaine 1987), modified to include the monopole component of the stellar disk. The stellar disk is realised using Jeans' equations with the potential of the disk and halo particles as computed by the EXP Poisson solver. The profiles are Milky-Way like: the dark halo is an NFW (Navarro et al. 1996) profile with $c = 15$ and $R_{vir} = 300$ kpc and an exponential stellar disk with scale length of 3 kpc and scale height of 350 pc. The stellar-mass to dark-matter ratio is 1/15. In both cases, the cold gas disk is initially in local hydrostatic equilibrium with a temperature of 3000 K based on numerical solutions of the one-dimensional Euler equations. For the Milky-Way like model, the gas disk has the same scale length as the stars and is rotationally supported. We do not include a separate bulge or spheroidal component in this model.

As described in Paper 1, these tests use an LTE cooling approximation rather than the full cross-section based Monte Carlo simulation of the Boltzmann collision term to facilitate a comparison with most of the published work on the subject. This model (Black 1981) includes atomic processes only so that temperatures lower than 3000 K will be of little energetic consequence. We will describe gas whose temperature is at the minimum of the cooling curve 'cold' gas. Use of the full DSMC method allows gas of any chemical composition and excitation state, and this will be studied in a later contribution (see Section 5 for additional details). The hot halo used in Section 3.6 is realised for simulation solving the hydrostatic equilibrium equation for the monopole term of the total gravitational potential fixing the temperature to $T = 10^6$ K and the density at the solar cir-

cle to $n = 10^{-4}$ atom/cc. The wind is realised as a uniform column with $T = 10^6$ K and $n = 10^{-3}$ atom/cc, initially moving toward the galaxy with a uniform bulk velocity of $2 \times V_{vir} = 240$ km/s. This modest wind velocity is low compared to that expected in a large cluster investigated by some authors (see Section 4). However, the momentum and energy of the wind is carried by particles in a DSMC simulation. Therefore, simulating a high-velocity wind requires a large column particles. This is computationally expensive, so we compromise with a wind speed more typical of a group interaction to lengthen the duration of the interaction. We explore three wind directions relative to the rotation axis of the disk: 0, 45 and 90 degrees. Once more than approximately 75% of the column has passed the galaxy, the simulation is terminated. The duration of the simulation, then, is approximately 400 Myr in our physical units.

The code is heavily instrumented, accumulating the mean Knudsen number, comparing the mean ballistic trajectory to the cell size, collisions per simulation particle, fraction of particles and cells in the EPSM limit for every cell at every time step. The mean velocity field, $\langle \mathbf{v} \rangle$, is characterised by gridding the gas particles and computing streamlines by numerically solving the first-order differential equations for the flow: $\dot{\mathbf{x}} = \langle \mathbf{v} \rangle$. Other mean quantities of the flow such as energy and angular momentum fluxes are readily computed from the gas particle distribution. These ensemble diagnostics will be used to illustrate the field quantities in the following sections. However, unlike hydrodynamic simulations, the particles in a DSMC simulation are *not* tracers of the underlying fields but carry the intrinsic quantities of the microscopic physical state of the gas. The computation of ensemble quantities, then, artificially degrades the true resolution of the simulation. In fact, the gas dynamics in the simulation takes place on a scale much smaller than the ensemble grid scale, often by an order of magnitude. For scenarios with unsteady flow, an accurate spatial ensemble estimate requires averaging over multiple simulations.

We will use two sets of units in this paper: 1) *system* units that assume that the mass and length of the entire bound system along with the gravitational coupling constant is unity; and 2) *Milky Way* units that scale the model to our Galaxy using physical units—kiloparsecs, years, and km/s. When quantities are quoted without units, they refer to *system units* and when quantities are physical units, they refer to *Milky Way* units.

3.3 Slab model: simple experiment

The first experiment is that of a one-dimensional slab of stars whose gravity confines a cool gas layer. This was designed to explicit test the Gunn-Gott criterion in its natural domain of validity: a wind impinging on a cold gas layer that is gravitationally confined to a plane-parallel slab. The stars have the classic isothermal distribution $\rho(z) \propto \text{sech}^2([z - z_{centre}(t)]/h)$ with scale height h and this distribution is fixed for all time. However, the centre of slab, z_{centre} , varies to conserve total linear momentum for the entire system. The gas is initialised in isothermal equilibrium with the confining slab with $T = 1000$ K and mid plane density of $n = 1$ atom/cc. The isothermal solution results in a gas scale height of approximately $0.3h$. The boundary conditions are periodic in the plane of the slab (x and y

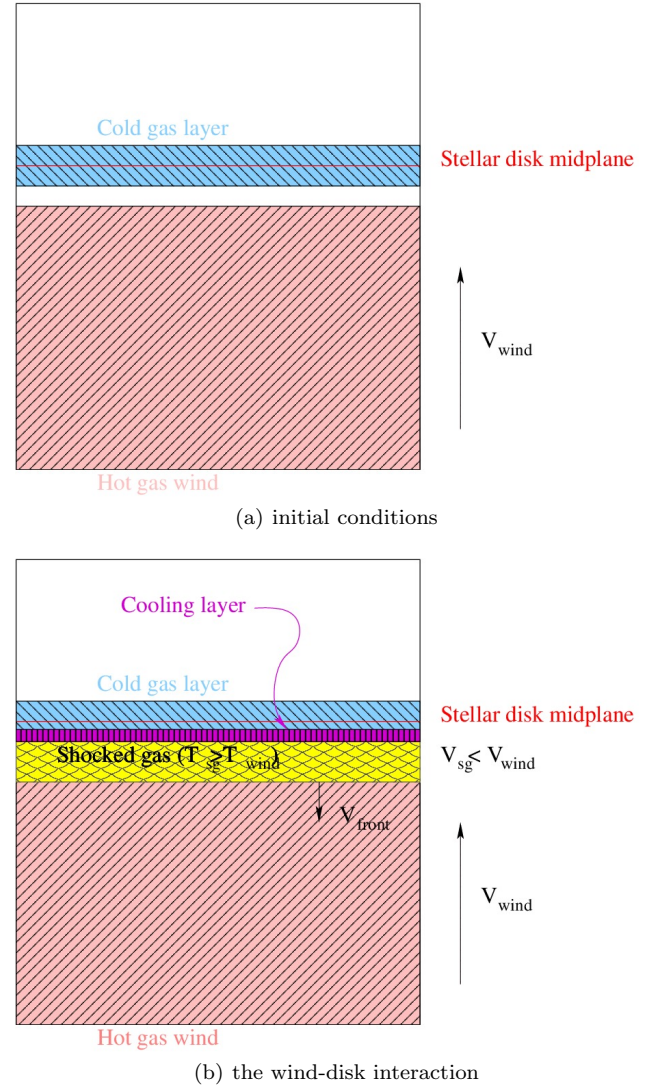


Figure 1. Description of the initial conditions (a) and the evolving hot-wind–cold-disk interaction (b) in the frame comoving with the disk. The cold and hot gas is indicated by blue and red shading respectively. In addition, the post-shock gas is shaded yellow and an enhanced cooling layer at the hot-cold interface is shaded purple.

directions) and vacuum in the vertical (z) direction. The simulation begins with a hot homogeneous wind ($T = 10^6$ K, $n = 0.001$ atoms/cc) filling the region $z < -10h$ with a mean vertical velocity chosen to exceed the Gunn-Gott criterion by a factor of three. As described above, all gas components may cool by atomic and plasma cooling mechanisms following the standard LTE cooling computation. See Figure 1(a) for a schematic description.

Much to my surprise, the cold gas does not escape the disk potential! Rather the evolutionary scenario is as follows. The gas shocks as it approaches the disk. The shock heats the gas, and the upstream compression wave propagates back into the original wind. When cooling is included, this shock stalls. The velocity of the turbulent, denser cooling layer of the post-shock hot gas is lower than v_{wind} and the pressure begins to displace the cold layer from mid plane. The momentum from the wind is transferred to the bulk

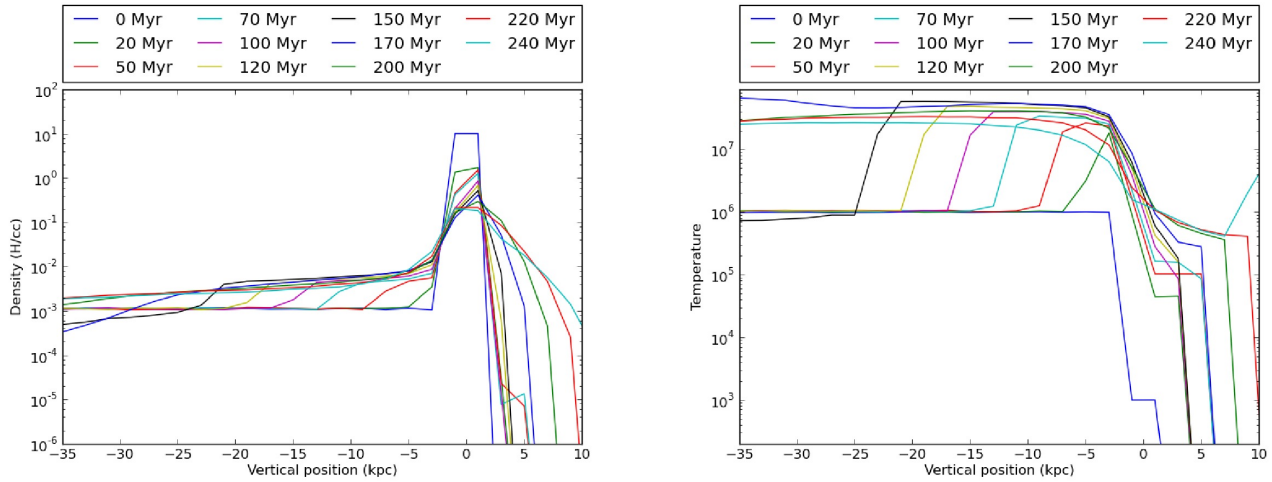


Figure 2. Evolution of the gas density (left) and temperature (right) for hot-wind–cold-disk interaction without cooling centred on the midplane of the stellar disk, $z_{centre}(t)$. The horizontal offset from the stellar midplane is shown in kiloparsec and the density scale is in H atoms per cubic centimetre (H/cc).

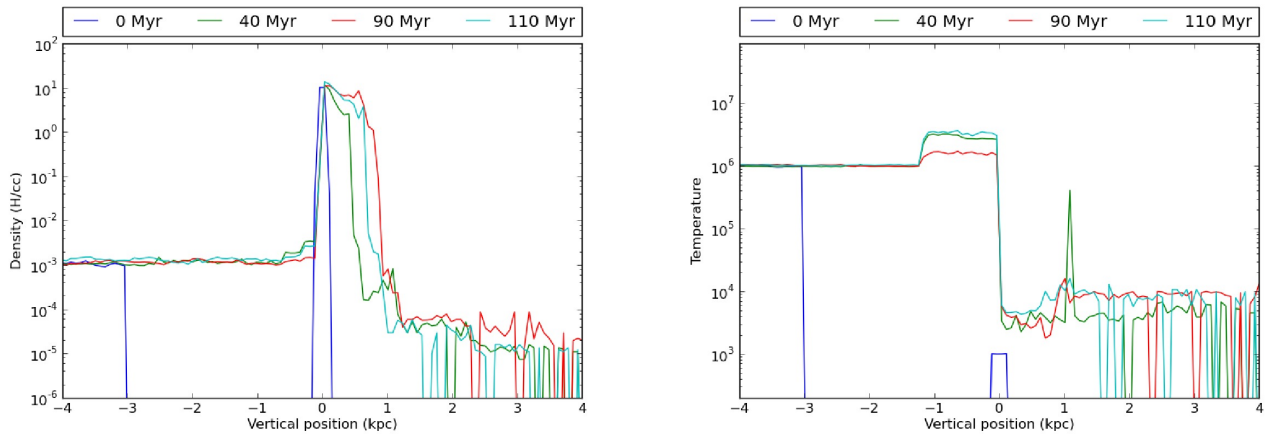


Figure 3. Evolution of the density (left) and temperature (right) for hot-wind–cold-disk interaction, as described in Fig. 3, but *with* atomic and plasma cooling. The horizontal scale as been zoomed to the much smaller region containing the response. The jagged distribution at $z \gtrsim 1$ kpc owes to binning variance caused by the very small mass of gas above the disk.

ISM through a cascade of primary and secondary inelastic scattering events. See Figure 1(b) for the location of these regimes. Furthermore, the hot gas begins to pressurise the cold gas, exciting two-phase instabilities that give rise to temperature and density ‘fingers’ as the 10^6 K gas displaces the volume originally occupied by the cold gas (not shown here). We will see in Section 3.4 that this production of multiphase features is enhanced by rotational shear. The total momentum is conserved but the slowed, compressed flow downstream of the shock implies that the wind does not transverse the disk on a ballistic crossing time. Rather, the slowed flow of hot gas increases the effective interaction time and allows the stellar disk to respond dynamically to the displaced cold disk. Then, the hot wind’s momentum is transferred to the stellar disk gravitationally. So in the end, the cold gas layer is not lost but rather the entire disk, gas and stars together, is accelerated, albeit weakly.

Figures 2 and 3 show the density and temperature state perpendicular to the disk plane with time. We begin with the evolution of density and temperature without gas cooling (Fig. 2). The curves at time 0 are the initial conditions. Without cooling, the energy deposited by the wind is sufficient to heat the initially cold gas layer to 10^6 K in 200 Myr. In this case, the shock forms and propagates upwind without stalling. The post shock wind gas increases its density (temperature) by approximately a factor of 4 (10). The dense initially cold gas is able to radiate a large fraction of deposited energy. After approximately 200 Myr, the now heated low-density disk component begins to flow downstream. Although this result agrees with the Gunn-Gott prediction, the mechanism is different: evaporation rather than impulsive momentum transfer.

The addition of radiative cooling qualitatively changes the ram-pressure response as shown in Figure 3). Three bins

cover the initially cold disk (red). On impact, the cold disk heats to approximately 10^4 K and thereafter radiates much of the wind-deposited kinetic energy. The shock forms, begins to propagate upwind, and stalls. The ISM reaches a new approximate thermal equilibrium between the kinetic heating and radiative cooling at approximately 10^4 K. The gas density decreases while the scale height of the initially colder gas increases. The distribution of the disk gas is skewed relative to the midplane determined by the stellar component but very little gas escapes.

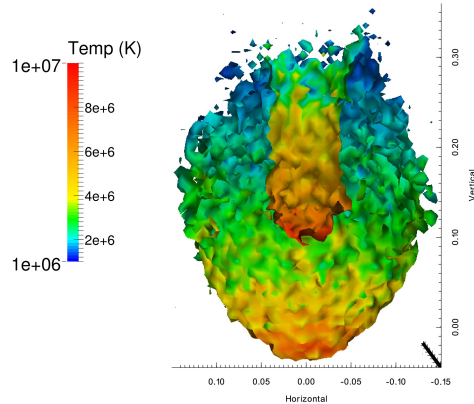
In summary, the scenario described in Section 2.2 failed to describe the flow because the momentum transfer is *not* in the impulse limit as derivation of equation (4) assumes. Owing to the shock, the post shock gas acts as a slowing moving piston. This gives time for the stellar disk to respond gravitationally to the displacement of the cold disk from the stellar mid plane. As a result, the initially cold gas layer is decelerated by the stellar disk causing the momentum from the wind to be transferred to the disk, and in the long run the entire system, although the disk-halo interaction occurs on a much larger timescale than in this simulation. Cooling is an essential ingredient that prevents the cold gas disk from evaporating. Without cooling, the disk gas is eventually evaporated, however with cooling, very little gas escapes.

3.4 Galaxy model: harder experiment

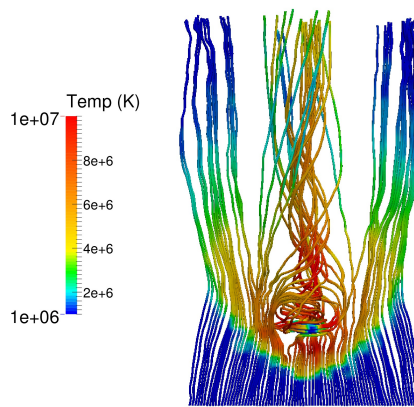
The first experiment was intentionally idealised and designed to check the Gutt-Gott mechanism in the simplest conceivable scenario. Intuitively, the inhomogeneity in the galaxy density profile will change both the downstream flow patterns and possibly entrain cold gas. How will this change the simple scenario above from Section 3.3?

To test this, we use the more realistic equilibrium galaxy model with the same wind column as in the previous experiment. The wind is only distributed in the vicinity of extended disk to best use computational resources as described in Section 3.2. Wind particles are not created during the simulation, and this results in wind-disk interaction event of limited duration; when most of the wind particles have reached the disk, the interaction is over. To prevent the adiabatic expansion of the wind column perpendicular to the flow, the gas is subjected to periodic boundary conditions in the two perpendicular directions. The duration of the simulation then is limited by either (i) the complete passage of the wind column past the galaxy or (ii) the wrapping of the flow transverse to the wind direction, whichever happens first. The vertical extent of the wind column is chosen, empirically, so that these two conditions obtain at approximately the same time. For simulations here, this is approximately 500 Myr after the wind impact, scaled to a galaxy of Milky-Way size.

Vertical slices containing the geometric centre of the disk through the gas density and temperature fields constructed from the ensemble values of the DSMC particles are shown in Figures 4 and 5. The initial condition, just before the vertically moving wind reaches the disk is depicted in the top-left panels of Figures 4 and 5. The disk plane is initially at $z = 0$. As in the simple slab model, the wind gas shocks as it reaches the galaxy. Initially, the momentum of the wind atoms is transferred directly to the cold gas. However, after the shock forms, the momentum



(a) isodensity surface



(b) streamlines

Figure 6. Density and streamline rendering of the gas flow at the same point shown in the last frame of Fig. 4. Panel (a) show a level-set surface corresponding to gas density of 0.003 particles/cc. This surface is approximately cylindrically symmetric, but has been cut by a vertical plane passing through the axis of symmetric to reveal its structure: a hollow sheath with the shape of a hornet's nest beginning with the bow shock at the bottom which a large narrow downward dimple corresponding to the inner sheath. The surface is colour coded by temperature, showing that the inner sheath is nearly 10^7 K as it leaves the disk. Panel (b) shows the stream lines colour coded by the temperature scale. The inner sheath is bounded by spiraling stream lines whose rotation comes from the angular momentum of the cold disk gas.

from the incoming wind is transferred by the shock to the slower, compressed downstream flow. The heated post-shock gas slows and piles up, increasing its density and driving a compression wave upstream into the wind. After approximately 100 Myr (the lower-right panels in Figs. 4 and 5), a well-defined Mach disk has formed with a temperature of close to 10^7 K, offset approximately 0.02 units below the disk plane (approx. 6 kpc, scaled to the Milky Way). Meanwhile, the hot wind begins to flow around the disk, heating and ablating the outer initially cold disk gas. Most of the disk gas is *ablated* at approximately 3 disk scale lengths. The temperature of the ablated gas is approximately 8×10^6 K.

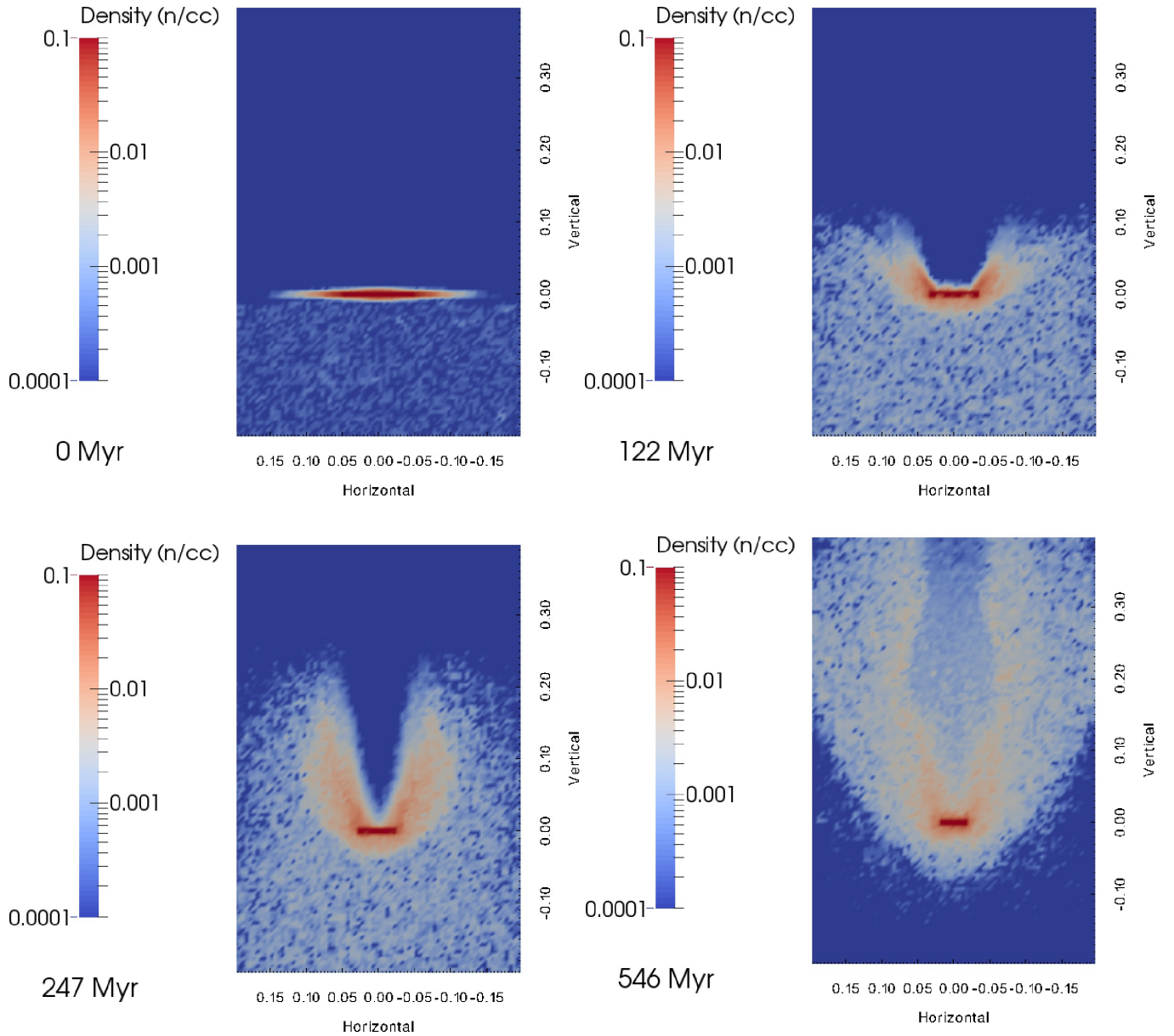


Figure 4. Edge-on view of the combined hot-wind–cold-disk gas evolution. Each panel describes the density in units of hydrogen atoms per cubic centimetre. One length unit is approximately 300 kpc scaled to the Milky Way galaxy. The elapsed time is inset in the lower right-hand side of each panel. The flow is cylindrically symmetric on large scales. The cold, dense disk is seen between $z = -0.01$ and 0.01 (wind direction) and $x = -0.04$ and 0.04 (transverse direction). The notches of lower density in the disk gas are due to strong two-phase instabilities.

This gas cools to approximately 4×10^6 K as it expands and forms a bell-shaped sheath.

Between 150 to 300 Myr after the initial impact, the gas continues to flow around and ablate the cold disk. The post-encounter wind mixed with the ablated gas forms a hot sheath. Owing to the angular momentum of disk gas ablated from approximately 3 disk scale lengths, the sheath has positive angular momentum with respect to the cylindrical axis. The unshocked wind, flowing around the galaxy, pressurises the sheath but the inward motion toward the symmetry axis is halted by its angular momentum barrier. This results in a relatively empty hot central core (final panel of Fig. 4).

By 300 Myr, the hot post-shock gas at impact param-

eters smaller than 2 scale lengths has begun to push itself through the cold disk. This has three consequences: 1) the additional pressure provided by the hot gas drives a strong two-phase cooling instability; 2) as the hot gas is pushed through the hot holes created by the instability, it receives some of the angular momentum of the cold gas. This flow is now partly rotationally supported against inward radial motion, creating a second inner sheath. Inside this sheath, there is only a hot tenuous gas with a much lower gas density than that of the initial wind (by approximately an order of magnitude); 3) the shear created by the vertical oozing of the hot gas through the now clumpy cold-gas layer excites a

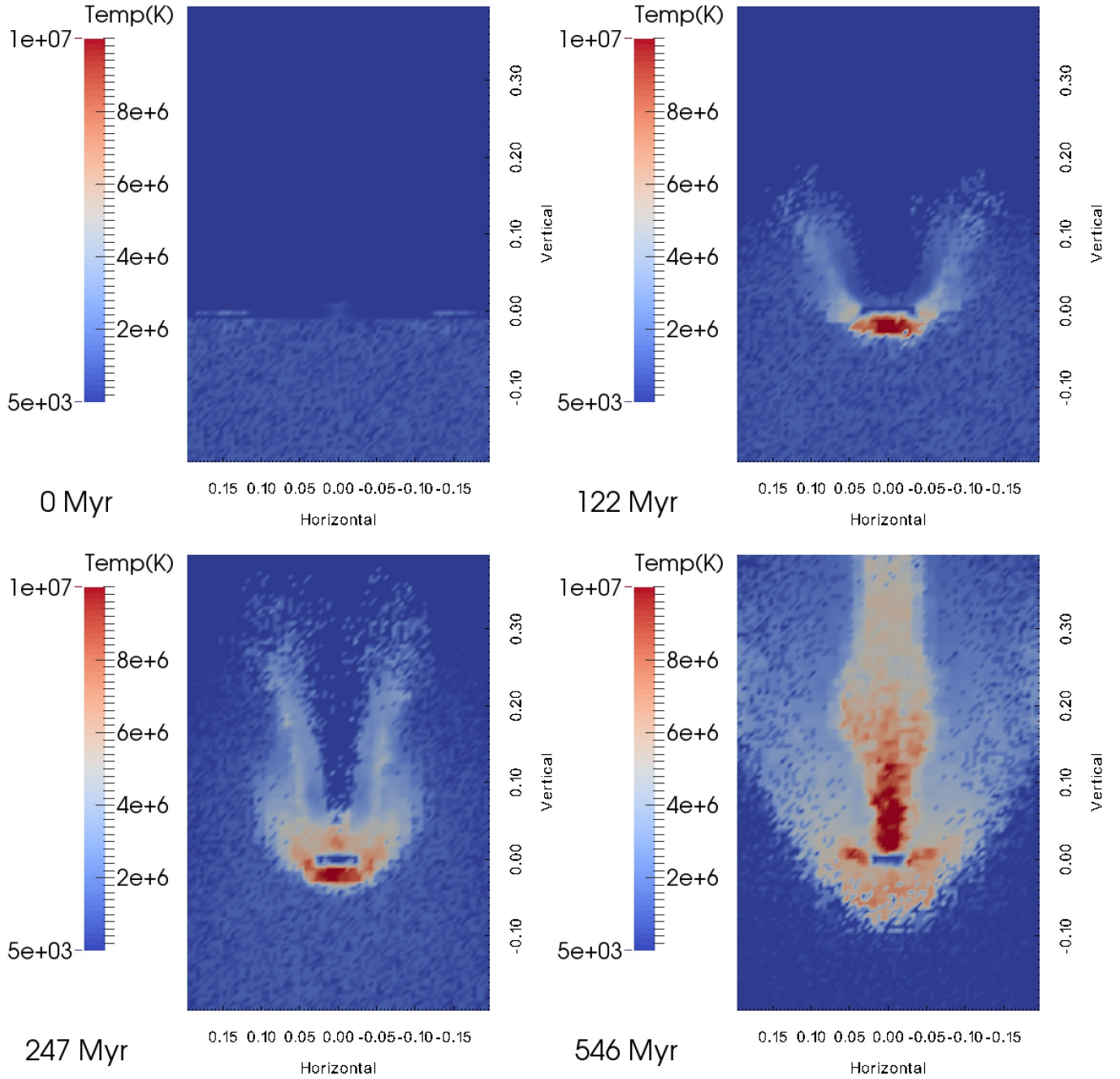


Figure 5. Edge-on view of the combined hot-wind-cold-disk gas evolution. Each panel describes the temperature in degrees K. The cold gas disk and the hot Mach disk are clearly seen at $z = 0$ and $z = -0.02$, respectively. The hot 'plume' visible between $z = 0.01$ and 0.06 is actually a hot low-density sheath supported against radial collapse by rotation.

Kelvin-Helmholtz instability in the disk plane (this will be described in detail below).

The fully developed wind-cold disk interaction at the end of the simulation is described in the final panel of Figures 4 and 5. The final panel of each of these figures describes the flow at the end of the simulation ($t \approx 550$ Myr). The hollow inner sheath begins to propagate upward in a spiral owing to the net angular momentum obtained from the disk. The inner sheath is very hot ($T \approx 10^7$ K) but with low density ($\lesssim 10^3/\text{cc}$). Figure 6 further illustrates the state of the gas at 550 Myr. The upstream gas is gravitationally

focused toward the galaxy giving the isodensity contours a hornet's nest shape. Panel (a) shows a rendered surface at a constant density of 0.002 atoms/cc colour-coded by gas temperature in degrees Kelvin. At the bottom of the surface sits the Mach disk at a temperature of 8×10^6 K. The projected rectangular feature between $z = 0.1$ and 0.3 , $x = -0.05$ and 0.05 is the inner boundary of the sheath; you are seeing a cut through a low-density tube. Panel (b) depicts stream lines integrated through the gridded volume used to compute the ensemble field quantities, also coded by gas temperature. The location of the shock front is clearly seen by the sharp

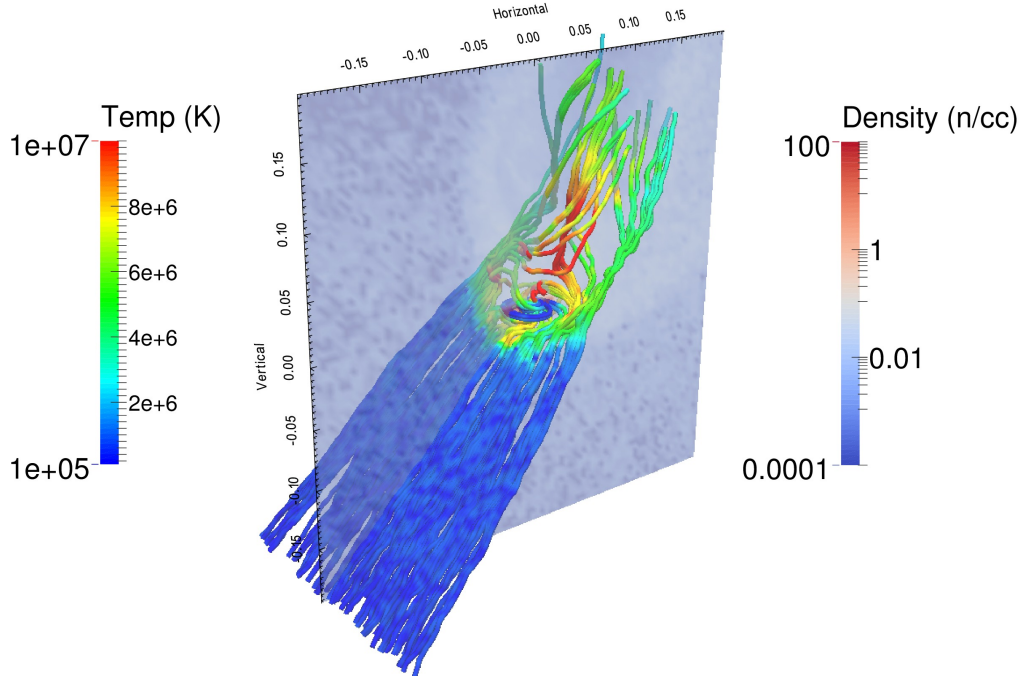


Figure 7. Streamlines showing gas flow for a hot wind with an impact angle of 45 degrees with a cold gas disk at 373 Myr after impact. The gas density of the flow in units of atoms/cc is shown on the translucent plane. The overall morphology of the flow is qualitatively similar to that for face-on impact.

jump in the temperature of the ambient wind gas from 10^6 K to $T > 4 \times 10^6$ K. After impact, the stream lines flare outward again and the gas cools a small amount. Approaching the inner galaxy, the hot gas attempts to push through the disk. In doing so, the hot gas gains some angular momentum and the cool gas loses some angular momentum. In the end, some net angular momentum is lost to the hot gas and the resulting spin can be seen in the streamlines. A small fraction of the low-density gas squeezes through the multiphase disk at small radii and small specific angular momentum to form a funnel of hot gas with $T \gtrsim 3 \times 10^6$ K.

This same numerical experiment has been repeated with a wind direction of 45 degrees to the disk normal direction with very similar results. Figure 7 describes the resulting flow with temperature-coded stream lines, as in Figure 6 with a density field slice along the symmetry axis. The stream lines and density slice reveal the same inner and outer sheath morphology as Figure 6. The cold disk response and the angular momentum transport are also quite similar to the face-on case, to be described below, so we will not consider the details of the oblique-wind simulation any further.

Typical of the galaxies with strong ICM interactions described in Chung et al. (2009), NGC 4522 shows little HI in the outer disk. Even more remarkable is the appearance of some gas above the inner disk, consistent with our prediction that the hot gas will force itself through the hot phase of the two-phase unstable disk during the later phases of the interaction. The extent of the neutral gas provides a further interesting diagnostic for the ICM–ISM interaction. Our simulation predicts that ram-pressure stripped hydrogen will not be observable in its neutral phase (cf. Fig. 5)

owing to the heat provided by the shock and carried by the turbulent flow which rapidly heats the initially cold gas in the outer galaxy. There are some caveats: the ICM density used here is larger by an order of magnitude and the wind velocity used here is smaller by nearly an order of magnitude than those values appropriate for Virgo. Given the complexity of this interaction, a direct prediction should be made with the appropriate values. In addition, because this simulation does not include gravitation on small scales; it is possible that this simulation misses small scale cold-blobs forming from cooling instabilities. However, the pervasive shock heating suggests that HI tails detected in galaxies that also show evidence of ram-pressure interactions (e.g. Vollmer & Huchtmeier 2007) have lost their neutral gas through tidal stripping. Nonetheless, the morphology of gas in NGC 4522 is qualitatively similar to that seen in these simulations and certainly appears to be an ongoing wind-disk interaction as indicated by Vollmer et al. (2008). It is conceivable that both mass-loss mechanisms are occurring simultaneously in NGC 4330 (Abramson et al. 2011). The time scale for survival of tidally-lost neutral gas in the hot turbulent wake of the ICM–ISM interaction may be distinctly morphology dependent and will require further work. Future work using the full DSMC collisional implementation will yield detailed radiative diagnostics (see Section 5) which will help disentangle the mechanisms.

Figure 8 shows the azimuthally averaged distribution of the disk’s gas mass inside of a given radius (in kpc) and as a function of time (in Myr). We see that approximately 40% of the initial gas mass is lost, and this is mostly from the outer disk and in the first 300 Myr. As seen in Figures 4–5,

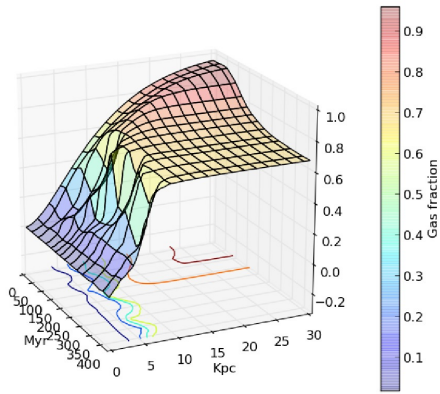


Figure 8. The cumulative fraction of gas in the disk with radius (in kpc) and time (in millions of years). The lower plane has been dropped below zero to reveal the contour lines.

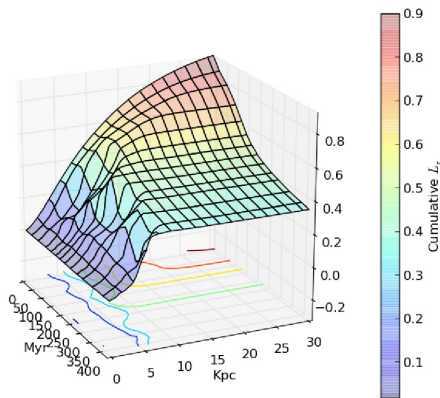


Figure 9. Similar to Fig. 8, this figure shows the evolution of the cumulative angular momentum fraction of gas in the disk with time. The contours on the base plane show fixed fractions for interpretive guidance.

the initially cold gas in the outer disk is ablated and heated. Although the gas continues to be ablated at a low level, the loss rate diminishes rapidly after 300 Myr owing to both the increased density of the cold gas after pressurisation and by the decrease in the scale length of the cold gas after its sizeable loss of angular momentum.

Figure 9 shows the evolution of the angular momentum fraction with time. This further emphasises that the disk gas is peeled off from the outside in and demonstrates that the overall gas content of the inner galaxy is largely unaffected. More than 60% of the original angular momentum content of the cold gas disk is lost to the wind, the dominant fraction owing to the mass loss. The wiggles in the constant angular momentum fraction contours are due to planar Kelvin-Helmholtz instabilities which we will describe next.

Figure 10 shows a sequence of density cuts through the disk plane. The density scale on the left of each panel describes the colour code for density in the range $n \in$

$[1.5 \times 10^{-5}, 1.5 \times 10^4]$ atoms/cc. The hot gas pushing through the cold disk from below picks up a small amount of angular momentum. This, in turn, creates a strong shear layer in the disk plane. This shear gives rise to a rampant Kelvin-Helmholtz (KH) instability. The KH waves develop and break, giving the familiar saw tooth pattern. The toothed ring then fragments: the inner parcels continue to move inward and the outer parcels move outward consistent with their specific angular momentum values. Gas from the destroyed ring coalesces into new rings and the process repeats. This limit-cycle behaviour is seen as saw-tooth-like wiggles in the angular momentum contours in Figure 9. At approximately 200 Myr into the wind-impact event, a stellar bar forms. The influence of the bar on the flow pattern is noticeable at $T \approx 300$ Myr.

The extent of the multiphase medium is shown in Figure 11 for the disk plane (top row) and the halo (bottom row). Recall from Paper 1 (Section 3.2.1) that the simulation code using a multiple time step algorithm. The left-hand column shows the gas after one major time step δT (25 Myr), chosen to allow the initial conditions to come to an approximate local equilibrium. The right-hand column shows the state of the gas after 200 Myr. These density-temperature plots show the classically expected two-phase instability (Field et al. 1969). The hot gas compresses the initially cold in the inner disk and shortened cooling time keeps it cold. The initially cold gas in the outer disk is warmed by the turbulent interaction with hot wind and this gas create the outer sheath. This results in the continuous distribution between the two phases in the figure. Note that this transitional gas only exists in the vicinity of the disk (top row); the sheath itself has $T \approx 10^6$ K (bottom row). Prior to the wind interaction, the T - ρ phase plane shows the hot tenuous wind and cold disk gas in two distinct and separated modes.

Figures 13 and 14 show the density and temperature for the gas at 100 Myr from the sequence in Figure 10. It is a particular moment in the non-linear evolution of the KH instability excited by shear created by the low angular momentum gas forcing its way through the disk. This particular snapshot shows a combination of coalesced rings connected by the spokes of the remnant KH instability. A detailed check shows that the hot and cold phases are in approximate pressure equilibrium. Moreover, the classic saturated KH instabilities are clearly seen on multiple scales (i.e. examine the saw-tooth shaped interface between the high and low density gas in these figures). Unlike previous figures that render ensemble-averaged field quantities, this figure shows individual gas simulation particles colour coded by their ensemble field values.

Finally, we may ask, are such things seen in Nature? I would argue that they are. For example, compare NASA/ESO image of the Cartwheel galaxy³ with the simulation profiles at 200 Myr (Fig. 15). Commonly, these rings and spokes are interpreted as a *splash* created by an intruder. A close look Cartwheel image galaxy reveals the same spokes and KH *scallop*ing seen in Figure 15 suggesting that the shear between hot wind gas and the cold disk gas is shaping the in-plane features! ROSAT and Chandra observations of the Cartwheel system reveal a stream of soft-

³ e.g. <http://chandra.harvard.edu/photo/2006/cartwheel1/>

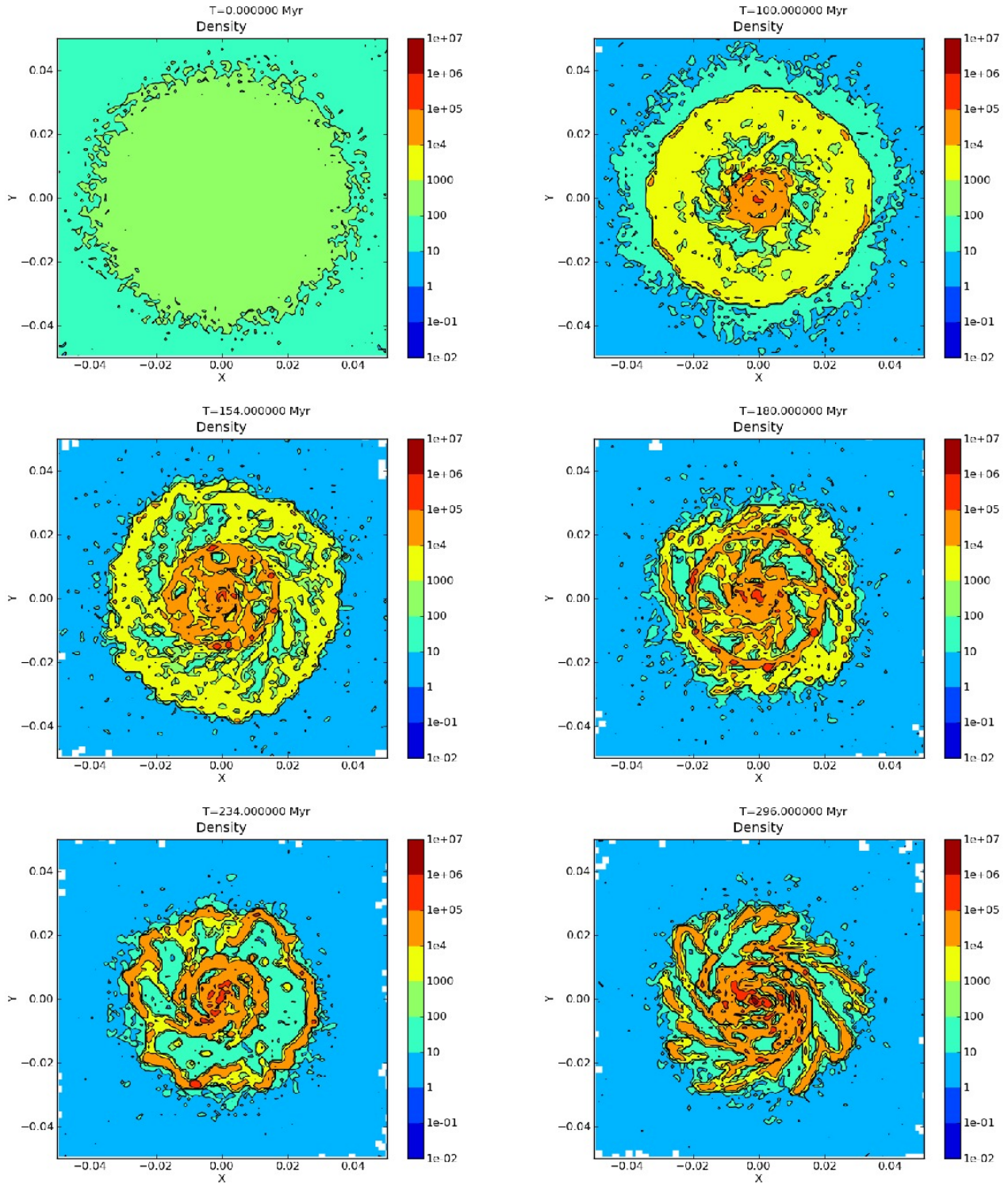


Figure 10. Gas density as a function of time (in system units) at the disk mid plane. System density units are 1.5×10^{-3} atoms/cm³ and one scale length is 0.01 system length units on the x and y axes. The time at the top of each frame is shown in millions of years (Myr).

x-ray emitting gas connecting the Cartwheel to its apparent companion intruders (Wolter & Trinchieri 2003) with an inferred column density of $N_H = 1.3 \times 10^{21}$ cm⁻². Assuming an outer ring diameter of 60 kpc, one estimates a hot gas

space density of roughly $n_H = 5 \times 10^{-3}$ cm⁻³, comparable to the wind densities in the simulations here.

Higdon (1996) estimated the expansion rate of the ring to be 53 ± 9 km/s based neutral H observations, consistent with the passage of an intruder approximately 300 Myr ago.

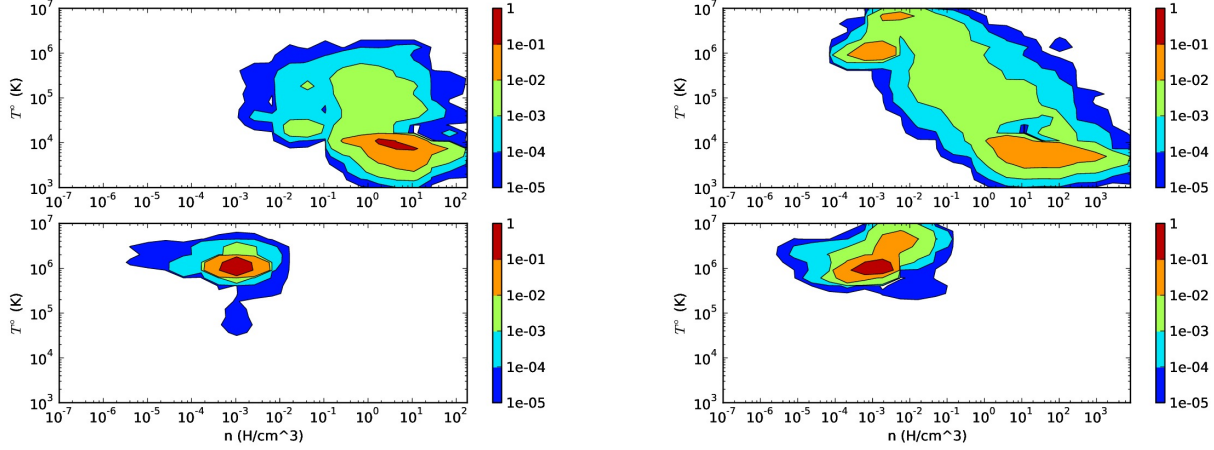


Figure 11. Density–temperature phase plane after 25 Myr (left column) and after 200 Myr (right column) for the initially cold disk gas (top row) confined to the region of the stellar disk, and the initially hot wind gas (bottom row), filling the region initially below but later above and below the stellar disk. The logarithmic colour scale denotes relative density on the phase plane. The initially cold gas develops a distinct hot tenuous phase through interaction with the hot wind (top row). Similarly, the hot wind is both heated and cooled through its interaction with the cold disk gas (bottom row).

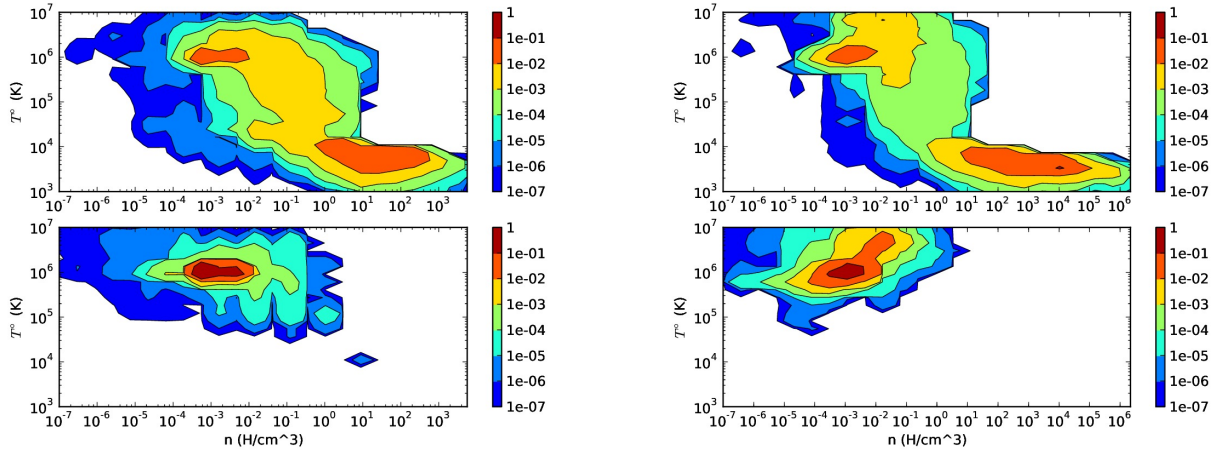


Figure 12. As in Fig. 11 but for the simulation including hot coronal gas initially.

Amram et al. (1998) estimated a mean expansion velocity of $13\text{--}30 \pm 10$ km/s with a superimposed sinusoidal distortion of amplitude 20 ± 5 km/s from $H\alpha$ observations. However, the expansion rate of the ring is similar to that found in the non-linear KH instability due to the wind. Altogether, it seems plausible that the observed spokes are not, as some have suggested, simply the original spiral arms of the target galaxy reappearing but the same KH instability seen in the simulations described here.

3.5 An edge-on wind

The affect of the edge-on wind differs qualitatively and quantitatively from that of the face-on wind. First, as might be expected, the shock forms in a rim around the outer cold disk, not like a Mach disk. The post-shock gas mixes with and ablates the cold gas. The angular momentum of the ini-

tially cold gas gives the flow some spin relative to the disk. The mixture of incoming wind and ablated cold gas moves around the disk in the direction of disk rotation. Approximately 70% of the cold disk’s initial angular momentum content is lost to ablation in this way. However, only approximately 10% of the cold disk mass is lost by 500 Myr after the encounter; this is nearly all of the gas outside of a radius 0.04 (12 Kpc in Milky Way units). Unlike the resulting disk in face-on encounter, there is little shrinkage of the inner disk.

At the same time, the hot wind flows under and over the disk and subsequently this gas is gravitationally focused on to the face of the disk. This, in turn, pressurises the cold disk and drives a strong multiphase instability. The pressure from the gravitationally focused wind is higher than from the Mach-disk-protected face-on wind leading to higher density in the cold gas phase. The phase-plane distribu-

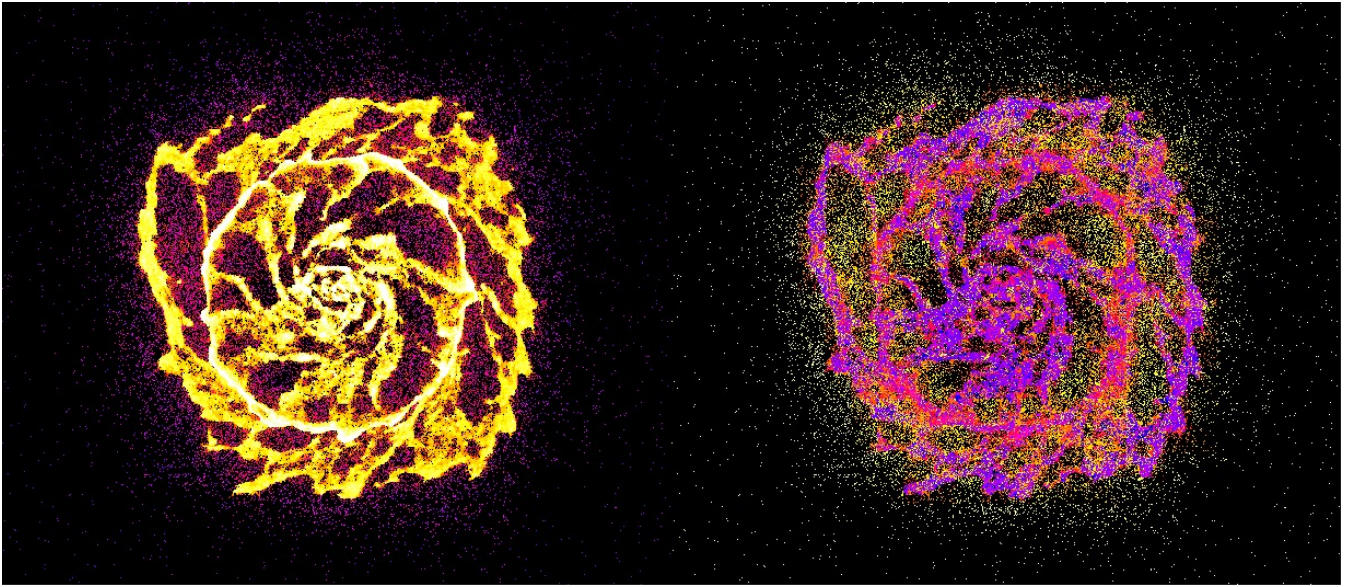


Figure 13. Cold disk from the simulation from Fig. 10 at 100 Myr. The left-hand panel shows gas density and the right-hand panel shows temperature. In both panels, the scalar is logarithmically mapped to a colour sequence that transitions from blue to red to yellow to white. On the left, the density of the hot gas (red) is 10^{-2} cm^{-3} and the density of the cold gas is 10^3 cm^{-3} . On the right, the hot gas (yellow-white) has $T \approx 10^6 \text{ K}$ and the cold gas (blue) has $T \approx 5000 \text{ K}$.

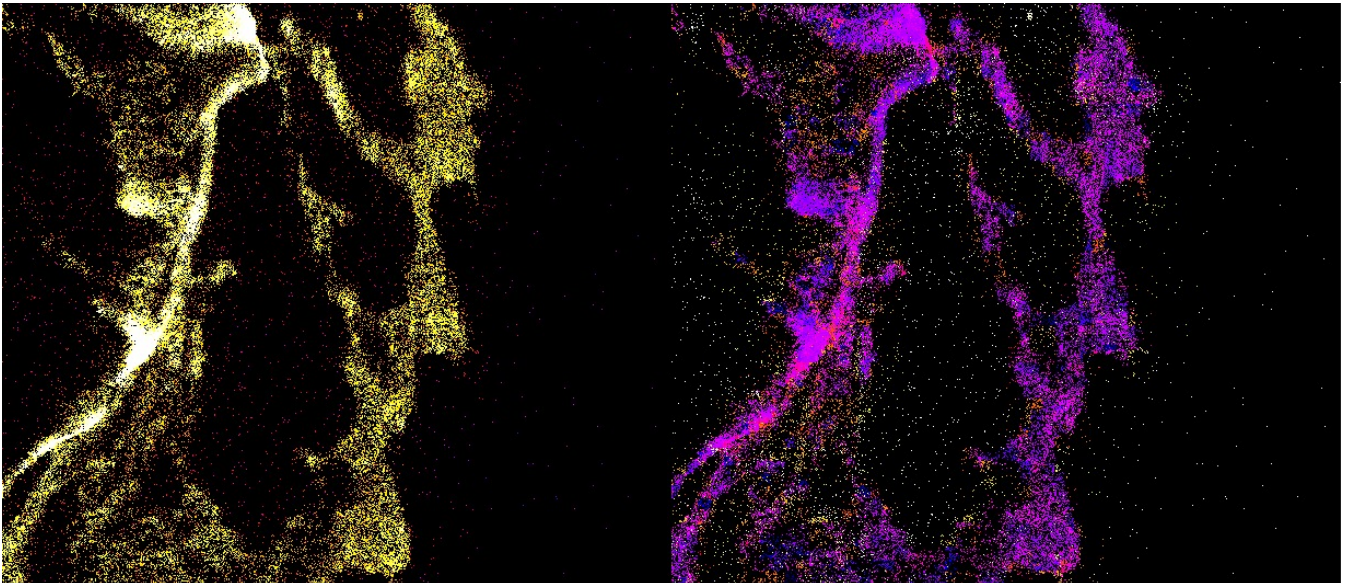


Figure 14. Cold disk at 100 Myr: close up. Panels and scales as in Fig. 13.

tion is similar to that for the face-on wind but very little of the gas has transitional densities and temperatures; the two phase remain well separated. In summary, although the overall outcome is similar to that of the face-on interaction, many features of the dynamical pathway to the final state are different.

3.6 The addition of coronal halo gas

To get some insight for the overall change in the wind–cold-disk interaction caused by a hot coronal halo, we repeat the simulation described in detail in Section 3.4 but adding

a hot isothermal coronal component in hydrostatic equilibrium in the galaxy with an initial temperature of 10^6 K and a density of 10^{-4} atom/cc at a radius of 30 kpc. This value was chosen to match typical hot halo densities estimated at large galactocentric radii. However, as described by Fang et al. (2013), this value may overestimate the inner galaxy density and underestimate the total coronal gas mass owing to the assumption of a cuspy, NFW profile.

The main results are as follows. The pressure from the hot-wind impact is more readily communicated through the coronal halo that is already in place downstream of the shock. This increases the pressure on the inner disk and

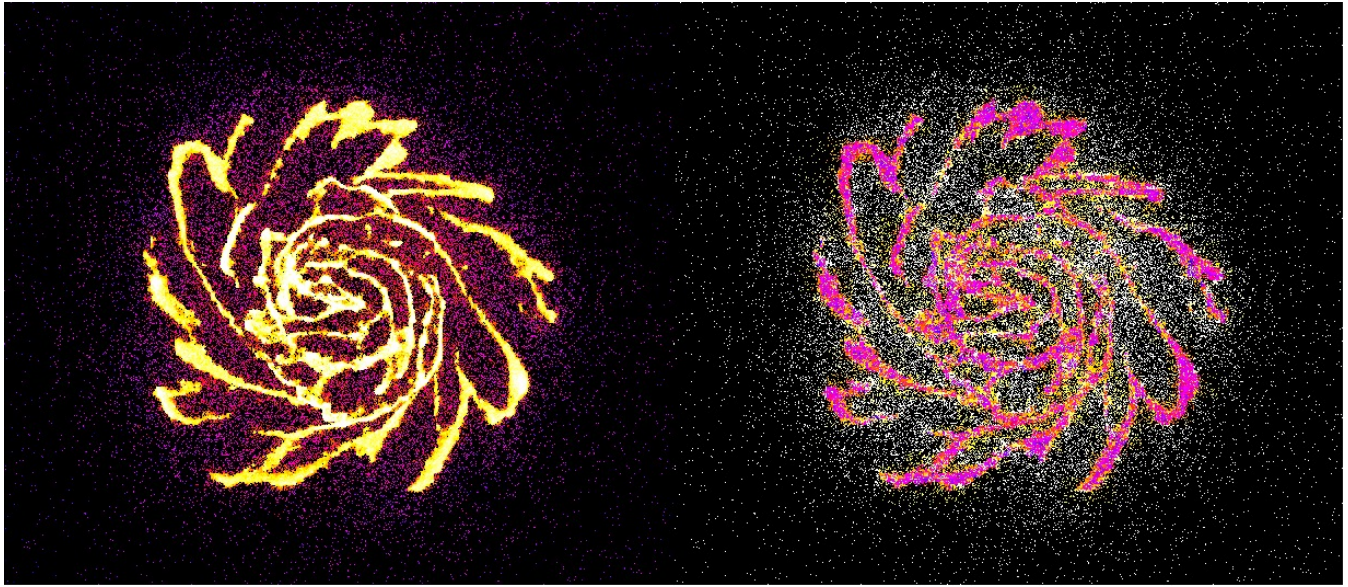


Figure 15. Cold disk at 200 Myr. Panels and scales as in Fig. 13. Note that the hot gas sits in the *void* opened up by shear in the cold gas. The saturation of the KH instability gives rise to rings and spokes, similar to those seen in ring galaxies. Moreover a close examination of the ring in the Cartwheel reveals the same sort of scalloping seen in the simulation shown here.

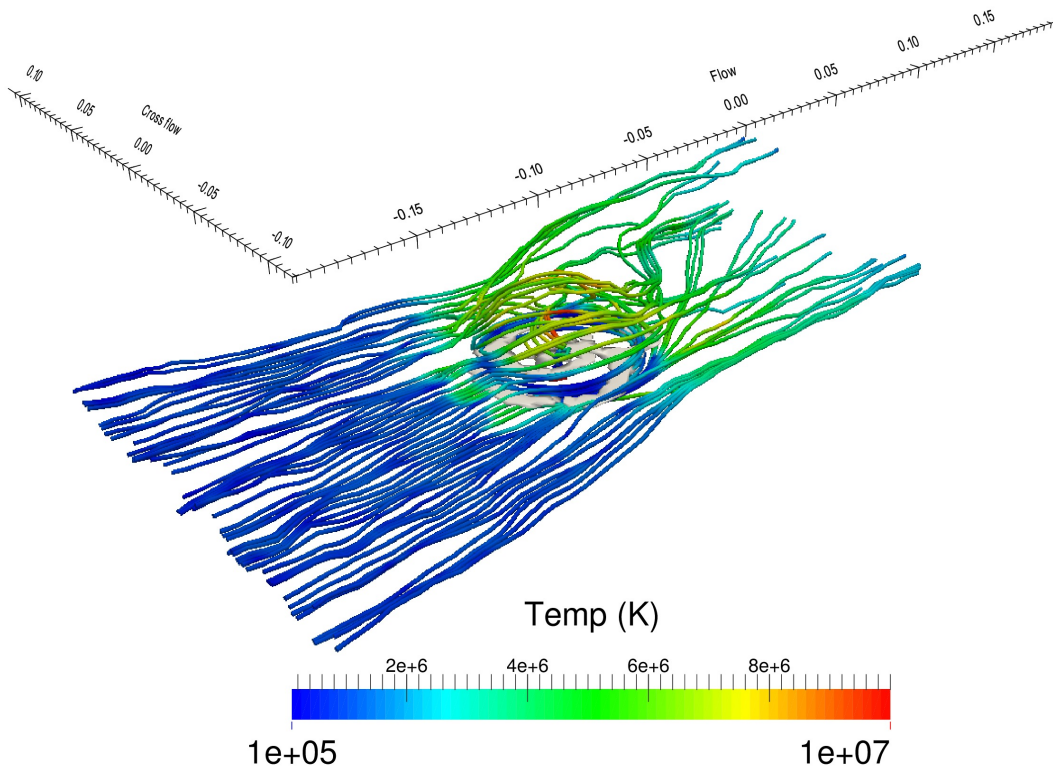


Figure 16. Streamlines showing gas flow for an edge-on impact of a hot wind with a cold gas disk at 400 Myr after impact. The wind flows from left to right in this figure and is colour coded by gas temperature (K). The gas density of the cold disk layer with density of 1 atom/cc is shown as the white surface. The up-stream gas is gravitationally focused toward the galaxy. The gas shocks on impact and the hot flow ablates the cold gas as in the face-on impact. Here, the ablated gas is pushed over or under the disk; through mixing, the mixture of the wind gas with disk gas gives the flow some overall rotation. Some of the hot gas is refocused down to the disk plane, heating the disk from above.

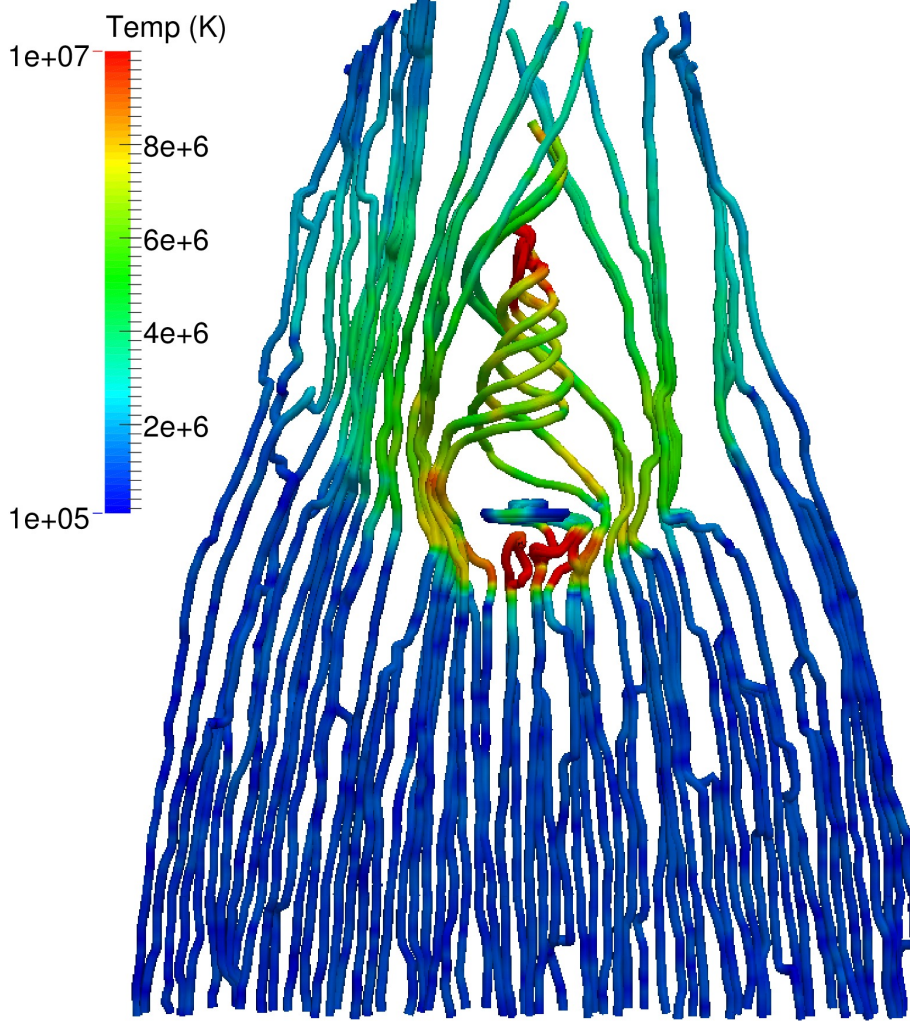


Figure 17. Similar to Fig. 6, streamlines showing gas flow for an edge-on impact of a hot wind with a cold gas disk at 250 Myr after impact. The flow is qualitatively similar to that without a corona. The main difference is the higher temperature of the downstream flow at small cylindrical radius.

results in a higher amplitude multiphase instability. This is seen through comparison of the density-temperature phase plane at the same interaction time with and without a corona (compare Figs. 11 and 12). Recall that the top row shows the gas in the disk and the bottom row shows the gas in the halo. The initial state in the vicinity of the disk reveals the superposition of the hot, hydrostatically-supported higher-density ($\gtrsim 3\text{H}/\text{cm}^3$) component peaking in the inner disk at and a lower-density ($\gtrsim 3 \times 10^{-2}\text{H}/\text{cm}^3$) component in the outer disk. Overall one sees more high density cold gas in the simulation with a corona. In addition, one sees that there is a smoother transition between the cold-dense and hot-tenuous phases in the flow without a corona; the corona suppresses the production of the intermediate-state gas by providing an additional heat source.

Similarly, the higher density of the hot gas at smaller galactocentric radii increases the angular momentum transfer from the cold disk to the post-interaction outflow by increasing the collisions of the hot, low angular momentum gas and the cool, high angular momentum gas. This is seen in the comparison of the cumulative angular distributions

shown in Figures 9 and 19. The total angular momentum drops nearly linearly to 10% of its initial value at 450 Myr after the initial impact. However, at the same time, the removal of this angular momentum causes the cold gas disk to shrink. This decreases the overall mass loss. In other words, the net result of the coronal gas is to *protect* the initially cold gas mass against stripping through ablation (compare Figs. 8 and 18). The disk loses only approximately 20% of its total mass overall, but by 450 Myr, all of this gas is inside of 8 kpc.

The overall flow pattern is the same with the hot corona (Fig. 17) and without (Fig. 6, lower panel). The extent of both the inner and outer density sheaths are smaller with the corona, consistent with larger angular momentum loss and disk shrinkage. Moreover, the simulation clearly shows that the density of the cool gas in the inner disk is much higher than without the coronal gas. The effect of the coronal gas on the inner galaxy may itself place a limit on the density of the inner coronal gas and thereby also place a limit on the shape of the galactic dark matter potential. This scenario is ripe for further investigation. Use of the non-LTE DSMC code,

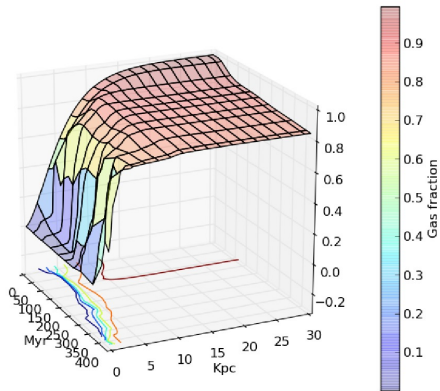


Figure 18. The cumulative fraction of gas in the disk with radius (in kpc) and time (in millions of years) for simulation with a coronal halo (cf. Fig. 8).

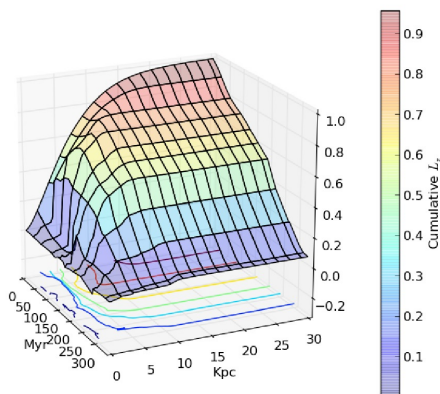


Figure 19. Evolution of the cumulative angular momentum fraction of gas in the disk with time for simulation with a coronal halo (cf. Fig. 9).

under development, will allow prediction of line-strengths for observed density and temperature diagnostic features (e.g. Mg II absorption).

4 DISCUSSION

The effect of ram pressure on galaxy morphology and transformation has been studied in several contexts over the last decade. A particularly nice example is provided by Crowl et al. (2005) who inferred the signature of ram pressure and ablation by combining optical, HI, and radio continuum observations for NGC 4402 (cf. Figs. 2 and 3 from Crowl et al. 2005). They argue that the absence of reddening at the disk’s edge implies truncation and that the position angle of linear dust filaments coincides with radio continuum, suggesting the ICM wind orientation. Similarly, Vollmer et al. (2008) show that observed regions of extraplanar gas with H- α flux have larger velocity than those with CO flux in Virgo galaxy NGC 4438, suggesting that the ionised gas is excited by the

ram-pressure mechanism. All in all, there is little doubt that ICM winds influence a galaxy’s ISM.

These and related observations have motivated a variety of computational hydrodynamic efforts and provide opportunities for comparison. The morphology of the flows in our simulations have the same morphological features as those performed with hydrodynamic codes (e.g. Bekki 2009, see his Figs. 2 and 7, using GRAPE-SPH). We expect DSMC to have lower resolution for the particle numbers used here than many of the hydrodynamic simulations discussed above, and therefore the good correspondence is encouraging. Also as expected, the interfaces between gas components and multiple phases are distinct, demonstrating a virtue of the kinetic approach.

However, since most authors had different sets of interests, goals, and physical choices, direct intercomparisons are often approximate. In addition to varied initial conditions, many used different equation of state combinations with and without atomic and plasma cooling. For some examples, Quilis et al. (2000) simulated the interaction between a spiral galaxy and the ICM of a rich cluster at a relative speed of 2000 km/s. They show that the interaction removes most of the gas in 100 Myr and argue that cooling is not important in this case. Our wind speeds are nearly an order of magnitude smaller than this, yet encouragingly, the morphological features of the ram-pressure response are very similar to those found here (see their Fig. 1). In contradiction, we conclude that the wind–disk interaction cannot remove all of the initially cold gas. However, we have not tried such a fast encounter; given the greatly increased energy and momentum content in this fast wind, it seems plausible that our result would be similar to theirs. Marcolini et al. (2003) and Mayer et al. (2006) performed hydrodynamic simulations of ram pressure stripping for dwarf galaxies. The former investigation considers winds typical of poor galaxy groups and considers the role of mass, velocity and wind direction. They find that dwarf galaxies may be stripped in a few hundreds of Myr (see their Fig. 4 for an illustration of the interaction morphology). Mayer et al. (2006) pattern their study on a Milky-Way-like system and consider the combined roles of ram pressure and orbitally induced tidal forces. Boselli et al. (2009) attempted galaxy evolution modelling with ram pressure and starvation. Their work suggests that anaemic spirals with truncated gas distributions and young populations have been produced by recent ram pressure event and cannot be produced by starvation alone. Similarly, they report that low luminosity dwarf disk galaxies can be transformed in dE galaxies with ease. Most of these are not directly comparable to the simulations described in Section 3.4 but they still exhibit many of the same morphological features qualitatively.

Many researchers compare their stripping results to the predictions of the Gunn–Gott criterion, although the general consensus is that this is only a crude approximation. In particular, as in this paper, a number of hydrodynamic simulations indicate an early phase of rapid stripping in the outer disk followed by a period of slower, viscous, stripping (e.g. Marcolini et al. 2003; Roediger & Hensler 2005). However, we demonstrate here that the initial mode of rapid stripping is ablation, not impulsive momentum transfer. Based on an extensive parameter survey, Roediger & Hensler (2005) develop a revised criterion based on pressure at the disk mid

plane. However, it is clear that the mass loss in the end depends on the widely differing ICM densities, velocities and galaxy mass (Bekki 2009).

In this study, our goal was the interaction physics itself rather than the implications for a specific astronomical scenario. In summary, although momentum is transferred from the wind to the disk ISM, the process bears little resemblance to its moniker, ram pressure, but rather seems to be an elaborate interplay between shocks, shear fronts, kinetic ablation (i.e. evaporation) and angular momentum transfer. Although it is natural to seek a scaling relation such as the Gutt-Gott criterion to summarise the overall outcome, the results of this paper suggest that an impulsive ram pressure approximation will be crude at best. The large variation of successes and failures of the criterion reported in the literature is not a surprise in this light.

Motivated by the discovery of a large ($M \approx 3 \times 10^8 M_\odot$) HI cloud in the Virgo cluster that appears to originate from the galaxy NGC 4388 (Oosterloo & van Gorkom 2005), Roediger et al. (2006) used hydrodynamic simulations to confirm that ram pressure is sufficient to strip this galaxy's gas mass. They report a distinctive flow pattern that they ascribe to von Karman oscillation, typically produced by the unsteady flow of a fluid past a blunt body, and suggest that the Oosterloo & van Gorkom (2005) discovery is evidence of this. The authors do remark that the observed HI tail morphology does not match the simulation and suggest that this discrepancy is due to missing physics and ICM interaction. We agree that this is likely. In particular, the results of this paper challenge the assumption that an adiabatic gas (Roediger et al. 2006) will correctly capture the nature of the mesoscopic interactions important at interfaces and that the hydrogen lost from the stripped galaxy will be neutral. As in the present work, Roediger & Brügger (2006) found that wind orientation angle does strongly affect mass loss unless the wind direction is nearly edge on.

Tonnesen et al. (2007) studied the problem from the Λ CDM galaxy formation and evolution viewpoint by tracking galaxies in clusters over time in a cosmological volume to ascertain the distribution of evolutionary drivers. They conclude that gas stripping is the most common mass loss mechanism and remains important out to the virial radius of the cluster. This general finding is consistent with our simulations. However, their aim was an ensemble survey using Λ CDM initial conditions. Given their limitations on resolution, a direct comparison with the details of the dominant physical mechanisms in their simulations is not possible.

Finally, Kapferer et al. (2009) explicitly investigated the dependence of star formation and morphology on the strength of ram pressure using combined N-body and hydrodynamic simulations with recipes for star formation and stellar feedback. They find that star formation is enhanced by more than a magnitude in the simulation with a high ram pressure relative to the same system evolving in isolation. They report that newly formed stars in the disturbed gas stars fall back to the old stellar disc, building up the bulge. They find also that gas stripping saturates quickly as in the simulations reported here. In addition, they describe a complex velocity pattern due to the rotation and spiral arms. This is qualitatively identical to the KH instabilities described in Section 3.4.

All in all, the simulations reported in this paper describe

similar features and mass loss fractions to those from hydrodynamic simulations when direct comparisons are possible. Moreover, our simulations underscore the importance of the interface in predicting the evolutionary morphology of ram-pressure induced flows and response. This suggests that the kinetic approach may become an essential tool for clarifying the dynamics of multiscale gas interactions for astrophysical flows.

5 SUMMARY

The ram pressure mechanism creates flows in multiply distinct gas phases with dynamically important interfaces, such as shock fronts and phase boundaries. Resolving the physics at these interfaces requires subtlety when using a hydrodynamic method but is naturally done by direct solution of the collisional Boltzmann equation using a kinetic-theory method. To this end, we explore the use of the hybrid kinetic theory–n-body code from Paper 1 to provide a check on our physical understanding of the ram-pressure scenario. The kinetic theory algorithm, Direct Simulation Monte Carlo (DSMC), is computationally costly, so we have not extensively surveyed the range of parameters relevant to all ICM–ISM interactions but rather focused on the dynamical mechanism for a single case, more typical of a group ICM density and velocity for a Milky-Way like galaxy (Free-land & Wilcots 2011). Overall, the findings from the simulations here are consistent with many of the previously published results. The simulations include a gravitationally self-consistent stellar disk, spheroid, and dark matter halo with an initially cold gas layer. The wind temperature is 10^6 K with a uniform bulk velocity set to twice the virial velocity of the galaxy initially. The choice of a group rather than rich cluster environment is partly motivated by computational expense. The key physical features of the gas response are as follows:

(i) The incoming wind shocks as it approaches the disk and a compression wave begins to propagate upstream. Meanwhile, the post-shock gas is heated, compressed, and this results in a lower bulk velocity in the downstream gas by approximately a factor of four. The ballistic crossing time of the hot gas is now close to the disk crossing time. The velocity of the hot wind gas decreases further as it pushes its way through the multiphase ISM.

(ii) The cold gas is not launched from disk en masse as in the impulsive approximation (Gunn & Gott 1972), but rather, the hot post-shock gas ablates and entrains the initially cool disk gas. The stripped gas ends up with a temperature close to that of the entraining wind.

(iii) The hot wind, either pushing through the disk for a face-on and oblique flow or impacting the disk from below and above for an edge-on flow, pressurises the cold disk and promotes a two-phase instability. The rapid consumption of gas by star formation and removal of the cold gas supply may well result in morphological transformations as previous authors have suggested. Indeed, Kapferer et al. (2009) and Tonnesen & Bryan (2010) find that gravothermal instability may promote cooling and star formation; our simulations neither include the molecular cooling or gravity on molecular cloud scales needed to investigate this possibility.

(iv) In the face-on or oblique wind–disk encounters, the post-shock ICM flowing through the now porous ISM has low specific angular momentum relative to the rotationally supported ISM. This results in a strong shear between the two phases with two important consequences: 1) the shear excites a strong Kelvin-Helmholtz instability that results in “ring and spoke” morphology; and 2) the hot wind carries off some of the gas disk’s angular momentum. This results in an inward advection of cold gas with the possible formation of an inner ring and a net rotation of the wind escaping the disk. The addition of angular momentum to the coronal plasma with the rotational orientation of disk may have interesting implications for galactic dynamos.

(v) Since the escaping gas is primarily lost from the outer disk, the outflow appears as a bell-shaped sheath for the face-on and oblique flows. The angular momentum gained through the interaction appears to help collimate the sheath by providing a centrifugal barrier at small radii. For an edge-on encounter, there is no well-defined inner sheath, although the cold gas disk casts a geometric shadow on the downstream flow creating a density dip along the flow axis.

In summary, we find that some initially cold gas does leave the galaxy as do most studies, but our simulations suggest that the process is complex. It is, therefore, unlikely to be shoehorned into a simple scaling law owing to the subtle dependence on initial conditions. The work here further suggests that the gas leaving the galaxy due to the wind interaction will be *hot* (i.e. not detectable as neutral hydrogen). We would need higher resolution and huge particle numbers to see the possible entrainment of small cold clumps or to resolve gravothermally unstable clumps. Furthermore, these simulations show that radiative cooling is critical to the flow pattern and cannot be ignored. Without cooling, most of the cold gas would heat and subsequently evaporate whereas with the cooling, we find strong multiphase instabilities that protect the gas against further large-scale mass loss. More generally, the phase and shock interfaces are likely to control the overall evolution of the gas and produce structure at all scales! Similar to collisionless dynamics, one can not gloss over interface regions even if their total volume is small.

Although DSMC was developed for high-Knudsen number (i.e. rarefied) flows, it may be used for near continuum flows as well. DSMC is more computationally expensive than traditional hydrodynamics for near-continuum flows, but has the advantage of unconditional stability, self-consistent momentum transport and no difficulties with formal discontinuities⁴. In particular, an ideally tuned DSMC simulation simultaneously maintains approximately 10 particles per simulation volume whose length scale is approximately 1 mean-free path. For denser flows, this condition is computationally infeasible. The implementation described in Paper 1 has a collisional limiter that transitions to the near equilibrium solution of the energy and momentum flux equations when the collision rate becomes very high. However, even in this limit, momentum and energy remain precisely con-

served and numerics of the flow remains stable. This makes DSMC ideally suited for investigating flows with momentum transfer and heating or cooling by conduction or radiation at interfaces.

Since this project arose as a code test, we have chosen to use an LTE approximation for gas cooling; this approach is also known as the *quasi static state* (QSS) approximation. QSS describes that collisional and radiative excitations as rates based on the local field quantities. In addition, we do not include electrons as a separate species for these simulations, but include their influence in the QSS limit. Therefore, electron conduction is not self-consistently simulated although hard-sphere conduction of the atoms is. On the other hand, a precise study of the excitations and electron interactions at the interfaces is necessary for estimating their physical state and dynamical influence on the flow. Moreover, accurate observational predictions depend on the state of the gas at the interface. It is precisely such investigation of interface dynamics and energetics on small and intermediate scales that motivated the combined DSMC–n-body code for transitional flows in the first place.

Therefore to improve the self consistency of these simulations, we are actively developing a version of our hybrid code that includes the full CHIANTI⁵ atomic database (Dere et al. 1997; Landi et al. 2011) for collisional cross sections and recombination (bound-bound and bound-free) and standard plasma transitions (free-free) for the ionised regime. This new implementation will allow us to straightforwardly make explicit predictions for both continuum and line-excitation strengths. However, it does not yet include the electrons as a separate kinetic species, but rather assumes that they follow the ions. This restriction will be relaxed in a future version that will allow a more realistic treatment of electron conduction and the dynamical influence of fixed magnetic fields. To be sure, simulation of these processes based on kinetic theory are very expensive but, in principle, will yield detailed observational predictions and accurate internal energetics and momentum transfer.

ACKNOWLEDGEMENTS

This material is based upon work supported by the National Science Foundation under Grant No. AST-0907951. I thank Aeree Chung for fascinating me with the perplexing dynamics of ram pressure physics.

REFERENCES

- Abramson A., Kenney J. D., Crowl H. H., Chung A., van Gorkom J., Vollmer B., Schiminovich D., 2011, *The Astrophysical Journal*, 141, 164
- Amram P., de Oliveira C. M., Boulesteix J., Balkowski C., 1998, *â*, 330, 881
- Bekki K., 2009, *MNRAS*, 399, 2221
- Binney J., Tremaine S., 1987, *Galactic Dynamics*. Princeton University Press, Princeton, New Jersey

⁴ In this sense, one might say that DSMC is 100% shock capturing, although more precisely DSMC has no need to *capture* a discontinuity because the physics of a shock front is resolved by the algorithm at the scale of the effective mean free path.

⁵ CHIANTI is a collaborative project involving George Mason University, the University of Michigan (USA) and the University of Cambridge (UK).

- Black J. H., 1981, *MNRAS*, 197, 553
- Boselli A., Boissier S., Cortese L., Gavazzi G., 2009, *Astronomische Nachrichten*, 330, 904
- Chung A., Van Gorkom J., Kenney J. D., Crowl H., Vollmer B., 2009, *The Astronomical Journal*, 138, 1741
- Crowl H. H., Kenney J. D., Van Gorkom J., Vollmer B., 2007, *The Astronomical Journal*, 130, 65
- Crowl H. H., Kenney J. D. P., van Gorkom J. H., Vollmer B., 2005, *AJ*, 130, 65
- Dere K., Landi E., Mason H., Monsignori Fossi B., Young P., 1997, *Astronomy and Astrophysics Supplement Series*, 125, 149
- Fang T., Bullock J., Boylan-Kolchin M., 2013, *The Astrophysical Journal*, 762, 20
- Field G. B., Goldsmith D. W., Habing H. J., 1969, *ApJL*, 155, 149
- Freeland E., Wilcots E., 2011, *The Astrophysical Journal*, 738, 145
- Gunn J. E., Gott J Richard I., 1972, *The Astrophysical Journal*, 176, 1
- Higdon J. L., 1996, *ApJ*, 467, 241
- Holley-Bockelmann K., Weinberg M., Katz N., 2005, *MNRAS*, 363, 991
- Kapferer W., Sluka C., Schindler S., Ferrari C., Ziegler B., 2009, *A&A*
- Landi E., Del Zanna G., Young P., Dere K., Mason H., 2011, *The Astrophysical Journal*, 744, 99
- Macrossan M. N., 2001, in *22nd International Symposium on Rarefied Gas Dynamics Vol. 585 of AIP Conference Proceedings*, A particle-only hybrid simulation method for near continuum flow. pp 388–395
- Marcolini A., Brighenti F., D’Ercole A., 2003, *MNRAS*, 345, 1329
- Mayer L., Mastropietro C., Wadsley J., Stadel J., Moore B., 2006, *MNRAS*, 369, 1021
- Navarro J. F., Frenk C. S., White S. D. M., 1996, *ApJ*, 462, 563
- Oosterloo T., van Gorkom J., 2005, *A&A*, 437, L19
- Pullin D. I., 1980, *J. Comput. Phys.*, p. 231
- Quilis V., Moore B., Bower R., 2000, *Science*, 288, 1617
- Roediger E., Brüggem M., 2006, *MNRAS*, 369, 567
- Roediger E., Brüggem M., Hoeft M., 2006, *MNRAS*, 371, 609
- Roediger E., Hensler G., 2005, *A&A*, 433, 875
- Tonnesen S., Bryan G. L., 2010, *ApJ*, 709, 1203
- Tonnesen S., Bryan G. L., van Gorkom J. H., 2007, *ApJ*, 671, 1434
- van der Wel A., Bell E. F., Holden B. P., Skibba R. A., et al., 2010, *arXiv preprint arXiv:1004.0319*
- Vollmer B., Braine J., Pappalardo C., Hily-Blant P., 2008, *Astronomy and Astrophysics*, 491, 455
- Vollmer B., Huchtmeier W., 2007, *Astronomy and Astrophysics*, 462, 93
- Vollmer B., Soida M., Chung A., van Gorkom J. H., Otmianowska-Mazur K., Beck R., Urbanik M., Kenney J. D. P., 2008, *A&A*, 483, 89
- Weinberg M. D., 2013, *MNRAS*, submitted
- Wolter A., Trinchieri G., 2003, *Memorie della Societa Astronomica Italiana Supplementi*, 3, 273